Journal of Power Sources 196 (2011) 355–360

Contents lists available at ScienceDirect

Journal of Power Sources

journal homepage: www.elsevier.com/locate/jpowsour

Structural transformation of Li_2CoPO_4F upon Li-deintercalation

Nellie R. Khasanova[a,*], Alexey N. Gavrilov[a], Evgeny V. Antipov[a], Kirill G. Bramnik[b], Hartmut Hibst[b]

[a] Department of Chemistry, Moscow State University, Leninskie Gory 1-3, Moscow 119991, Russia
[b] BASF SE, Ludwigshafen 67056, Germany

ARTICLE INFO

Article history:
Received 2 April 2010
Received in revised form 18 June 2010
Accepted 24 June 2010
Available online 1 July 2010

Keywords:
Lithium batteries
High-voltage cathode material
Structure transformation

ABSTRACT

Electrochemical performance and structural properties of the high-voltage cathode material Li_2CoPO_4F have been investigated. The cyclic voltammetry and coulometry under potential step mode in the voltage range 3.0–5.1 V vs. Li revealed a structural transformation at potentials above 4.8 V. This transformation occurring upon Li-extraction appears to be irreversible: the subsequent Li-insertion does not result in restoration of the initial structure, but takes place within a new "modified" framework. According to the structure refinement this modification involves the mutual rotations of (CoO_4F_2) octahedra and (PO_4) tetrahedra accompanied by the considerable unit cell expansion which is expected to enhance the Li-transport upon subsequent cycling. The new framework demonstrates a reversible Li-insertion/extraction in a solid-solution regime with stabilized discharge capacity at around 60 mAh g^{-1}.

1. Introduction

Rechargeable lithium-ion batteries are considered to be the most advanced energy storage system. Despite the commercial success of $LiCoO_2$ based lithium-ion batteries in portable electronic devices, high cost, toxicity and thermal instability prohibit its use in large-scale application. In an intensive search for alternative materials, olivine phosphate $LiFePO_4$ proposed by Padhi et al. has been shown to hold a particular promise [1]. Being both inexpensive and environmentally benign, $LiFePO_4$ exhibits rather high energy density, and demonstrates remarkable electrochemical and thermal stability if compared to lithium metal oxides [1–3]. These superior properties result from three-dimensional framework consisted of transition metal–oxygen octahedra interconnected with (PO_4)-group. Development of new synthetic approaches which allowed to turn this compound of poor electron and Li ion mobility in attractive cathode materials created a new trend in the search for new electrode materials, involving the investigation of framework compounds with different polyanions $(XO_4)^{m-}$ (X = S, P, Si, B) [3,4]. It should be noted that this class of materials benefits from inductive effect of polyanion group, which increases the redox potential of the transition metal element as compared to corresponding oxides [5,6]. Furthermore, the potential value can be "tuned" by varying X, and in attempt to enhance the electrode potential many Li-containing compounds, such as silicates, sulphate, borates, fluorophosphates and very recently fluorosulphate have been explored [7–14].

Framework compounds containing fluoro-oxyanions can be perspective as high-voltage cathode materials because a higher ionicity of the M–F bond (as compared to the M–O one) is expected to enhance the potential of the corresponding M^n/M^{n+1} redox couple. Several fluorophosphates have been shown to host mobile Li ions which can be reversibly extracted/inserted, and an increase of the electrode potential of the V^{3+}/V^{4+} couple as compared to $Li_3V_2(PO_4)_3$ was reported for the $LiVPO_4F$ and $Li_5V(PO_4)_2F_2$ fluorophosphates [7,10,11]. Fluorophosphates of general formula A_2MPO_4F (A = Li, Na and M = Fe, Mn, Co, Ni) crystallize in three structure types, which differ in the connectivity of (MO_4F_2) octahedra: face-shared (Na_2FePO_4F), edge-shared (Li_2MPO_4F, M = Co, Ni) and corner-shared (Na_2MnPO_4F) [12,15–17]. The Li_2FePO_4F fluorophosphate (isostructural to Na_2FePO_4F) was shown to be electrochemically active with a redox voltage at around 3.5 V and a reversible capacity of 0.85 Li per unit formula [12]. High-voltage electrochemical activity was reported for other fluorophosphate phase, Li_2CoPO_4F, though cyclic stability and sustained capacity of this material were not discussed [18]. Our previous investigation of the Li_2CoPO_4F phase and related compounds revealed the irreversible structure modification caused by Li-extraction indicating thereby the complex behavior of this fluorophosphate phase upon electrochemical cycling [19]. In this paper we describe the structural behavior of the Li_2CoPO_4F phase taking place on Li-insertion/extraction, and present a brief characterization of its electrochemical properties.

2. Experimental

The following chemicals were used as starting materials: Li_2CO_3 (99.1%), $FeC_2O_4 \times 2H_2O$ (99.9%), $(NH_4)H_2PO_4$ (99.4%), LiF

* Corresponding author. Tel.: +7 495 939 34 90; fax: +7 495 939 47 88.
E-mail address: nellie@icr.chem.msu.ru (N.R. Khasanova).

0378-7753/$ – see front matter © 2010 Elsevier B.V. All rights reserved.
doi:10.1016/j.jpowsour.2010.06.086

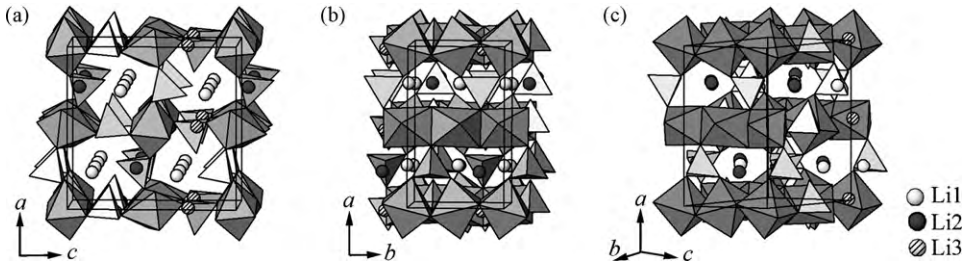

Fig. 1. Crystal structure of Li_2CoPO_4F: views along different directions a) [0 1 0], b) [0 0 1], and c) [0 1 1]. Transition metal octahedra and phosphate tetrahedra are shown; positions of lithium atoms are indicated.

(99.5%), $Co(NO_3)_2 \times 6H_2O$ (99.9%), $Ni(OH)_2$ (99.9%). Synthesis of fluorophosphates, Li_2CoPO_4F and $Li_2Ni_{1-x}Fe_xPO_4F$, was carried out by two-step solid state reaction. At the first step $LiMPO_4$ samples were synthesized. Appropriate amounts of initial reagents were grinded in a planetary ball mill for 2 h and pelletized. The samples were treated at 350–380 °C for 10 h and at 650 °C for 20 h with intermediate regrinding in the milling machine. Annealing was conducted under flowing Ar. The obtained $LiMPO_4$ samples were mixed with appropriate amount of LiF (ball milling for 2 h), pelletized and placed in a Ni-foil container. Then it was inserted in tube furnace set, annealed at 650–700 °C for 1–2 h under Ar-flow and subsequently quenched to room temperature. The carbon-containing composite, Li_2CoPO_4F/C, was prepared by adding a carbon black (5 wt.%) to initial mixtures; the level of residual carbon in the obtained composite was determined by thermal analysis and taken into account during preparation of electrodes.

Chemical oxidation (extraction of lithium) was carried out by stirring microcrystalline samples with nitrosonium nitrate, $NONO_3$, in acetonitrile solution for 20 h. Chemical lithiation of samples was performed using an excess of n-BuLi (1.6 M) in a solution of hexane. Reaction was maintained under constant stirring at ambient temperature in a flask kept in a nitrogen filled glove-box for 2 days. The obtained product was washed thoroughly with hexane and finally dried under vacuum.

The samples were characterized by powder X-ray diffraction (XRD) using a Huber G670 Guinier camera ($CuK\alpha_1$-radiation, Ge monochromator, image plate detector). XRD data for structure refinement were collected on a STOE-STADI P diffractometer ($CuK_{\alpha 1}$-radiation, Ge monochromator, linear position sensitive detector) in the range 10–100° (2θ) at 0.02° intervals. The material particle size and product morphology were examined by a scanning electron microscope "JEOL 6490LV" equipped with an energy dispersive X-ray spectroscopy (EDX) attachment. Thermal analysis was performed by thermo-gravimetric differential scanning calorimetry (TG-DSC) apparatus STA-449 (Netzsch, Germany). The particle size distribution was studied by a laser particle size analyzer Analysette 22 (Fritsch, Germany).

Electrochemical evaluation of the test materials was carried out in a hermetic cylindrical cell made of Pyrex-glass and consisted of three electrodes. The counter electrode was made from thick lithium foil, the glass tube filled with lithium metal and connected to current collector was used as the reference electrode. The positive electrode was prepared by thoroughly mixing of active material (71 wt.%), carbon black (19 wt.%) and PVdF (10 wt.%) in *N*-methyl-pyrrolidone. As-prepared ink was placed on the Al-foil support (area of 0.5–0.8 cm^2) with typical electrode loadings of 1–2 mg cm^{-2}. The prepared electrodes were dried in oven at 70 °C overnight, pressed (3.2 t cm^{-2}), then dried again for several hours at 80–100 °C under vacuum. The electrolyte was composed of a 1 M $LiPF_6$ solution in ethylene carbonate/diethyl carbonate/dimethyl carbonate (1:1:1, v/v/v). The measurements were performed under cyclic voltammetry and potential step modes with AUTOLAB PGStat 302 potentiostat and GPES Software. The *ex situ* XRD study of the tested electrodes were performed by covering the electrode with mylar film to avoid reaction with moisture/air.

3. Results and discussion

Synthesis of fluorophosphate, Li_2CoPO_4F was carried out by two-step solid state reaction. At the first step $LiCoPO_4$ with the olivine structure was synthesized. At the next step prepared $LiCoPO_4$ sample was mixed with appropriate amount of LiF, and obtained mixture was used for preparation of fluorophosphate phase. Preliminary investigation on synthesis optimization revealed the metastable nature of fluorophosphate phase. It was found that Li_2CoPO_4F is formed quickly (annealing for 1–1.5 h), while annealing for longer time (more than 1.5 h) results in decomposition of the fluorophosphate phase into $LiCoPO_4$ and LiF. Therefore short-time annealing and quenching were applied to produce single-phase Li_2CoPO_4F, which was obtained by heating at 700 °C for 1 h. To prepare the Li_2CoPO_4F/C composite the mixture of LiF and $LiCoPO_4/C$ was used, and sample without any contaminations visible on XRD pattern was obtained when some excess of LiF (0.2 M) and lower firing temperature (670 °C) were applied. For the Li_2CoPO_4F/C composite the average particle size determined by laser diffraction was about 0.6 μm.

According to XRD the obtained Li_2CoPO_4F phase is isostructural with Li_2NiPO_4F [10], its pattern is entirely indexed in *Pnma* space group with cell parameters $a = 10.452(2)$ Å, $b = 6.3911(8)$ Å and $c = 10.874(2)$ Å. As well as the olivine phase, it consists of a 3D framework. In contrast to the olivine structure with metal–oxygen octahedra connected through corners, Li_2CoPO_4F is built of edge-shared (CoO_4F_2) octahedra. Thus formed rutile-like chains are interconnected by (PO_4) tetrahedra to form the framework with channels occupied by Li ions (Fig. 1a and b). There are three distinct, fully occupied lithium positions with different coordination environments consisted of the two five-coordinated sites (Li1 and Li2) and one distorted octahedral one (Li3). The framework structure of Li_2CoPO_4F is expected to allow lithium-ion diffusion through a pair of extended channels (along the [0 1 0] and [0 1 1] directions), which are accessible to atoms located on the Li1 and Li2 positions. The first migration pathway along the *b*-axis is available to lithium ions at the Li1 site, while both Li1 and Li2 ions can approach the second one along the [0 1 1] direction (Fig. 1a and c). To differentiate Li ion mobility among three different lithium sites, bond valence sum (BVS) calculations were performed [20]. The BVS values were shown to be good indicators of easy-of-extraction of lithium ions from the structure [21]. According to BVS calculations lithium positions in Li_2CoPO_4F are inequivalent: 0.771 for Li1, 0.978 for Li2 and 1.22 for Li3. Thus, Li3 ions with shortest distances to the nearest neighboring oxygen/fluorine atoms (and with higher BVS value of 1.22) are more tightly bound and, therefore, less mobile. Lithium ions at the Li1 site (with much lower BVS value of 0.771) are the least tightly bound, and should be easily extracted upon charge. These BVS calculations together with the structure considerations give indirect support for facile transport of Li1 ions in compari-

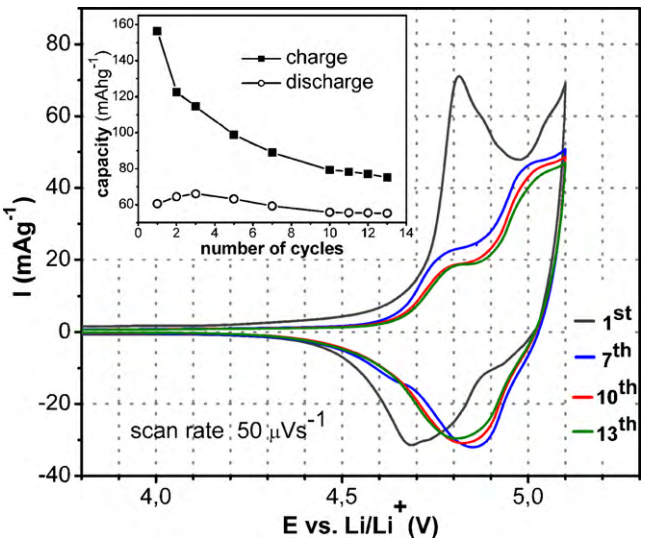

Fig. 2. Cyclic voltammograms measured with Li_2CoPO_4F electrodes in the potential range 3.0–5.1 V at the scan rate 50 $\mu V\,s^{-1}$ (number of cycles are indicated). The insert shows the capacity decay upon cycling.

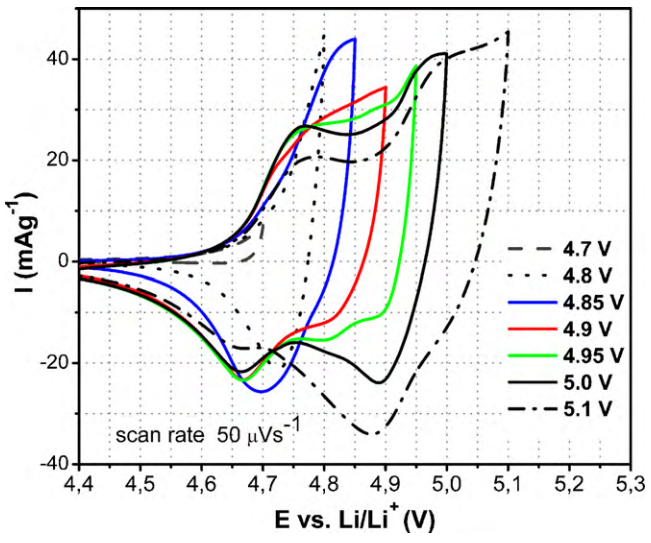

Fig. 3. CV curves with variable anodic limits (indicated) measured on Li_2CoPO_4F electrodes at the scan rate 50 $\mu V\,s^{-1}$.

son with Li2 ions, while the probability of diffusion for Li3 ions is expected to be rather low.

Cyclic voltammograms (CV) of the Li_2CoPO_4F electrodes were measured in the potential range 3.0–5.1 V at a scan rate of 50 $\mu V\,s^{-1}$. Upon the first charging the broad irreversible peak at 3.3 V was observed, and it disappeared completely upon further cycling. The subsequent CV curves (Fig. 2) revealed complicated nature of electrochemical processes occurring in the $Li//Li_2CoPO_4F$ cell, which in addition suffered from electrolyte instability at high potentials. Shapes and positions of the oxidation and reduction peaks were drastically changed in the initial cycles, and only after 7 complete cycles no pronounced modifications of CV curves were detected. For these "stabilized" curves, at least two oxidation peaks (~4.8 and 5.0 V) are recognizable on the charge branches, while corresponding reduction peaks at ~4.85 V are very broad and less resolvable. These potentials are close to the redox potential of the Co^{2+}/Co^{3+} couple found in the olivine $LiCoPO_4$ phase [22,23], confirming that the observed electrochemical activity should be assigned to the Co^{2+}/Co^{3+} redox couple. Furthermore, these results are consistent with the data on Li_2CoPO_4F reported by Okada et al. [18]. The insert in Fig. 2 shows the specific capacities of the Li_2CoPO_4F electrode estimated from CV curves (without background corrections). The considerable loss of charge capacity for the initial cycles can be attributed to side reactions caused by the electrolyte instability and the electrode passivation usually taking place at potentials close to 5 V (vs. Li/Li^+) [22]. Discharge capacity of ~60 mAh g^{-1} corresponds to insertion of about 0.40 Li (comparing with the theoretical capacity of 141 mAh g^{-1} for 1 e^- transferred). This value seems to be limited by the cutoff potential of 5.1 V (vs. Li/Li^+), since according to the shape of the CV curves electrochemical processes remain uncompleted at potentials around 5.1 V. However, higher anodic limit potentials were avoided because of destructive contribution of side reactions (e.g. charging up to 5.4 V resulted in the dramatic decay of electrochemical activity after 3 complete cycles).

To get insight of electrochemical processes CV measurements with various cutoff potentials (up to 5.1 V, with step of 0.05 V) followed by *ex situ* XRD experiments were undertaken. From CV curves with variable anodic limits (Fig. 3) it was proposed that processes taking place at potentials below and above 4.8 V are different or an additional process appears slightly above 4.8 V. This suggestion was supported by results of X-ray diffraction study. The *ex situ* XRD patterns taken for electrodes charged/discharged to different potentials are shown in Fig. 4. For the electrode that had been cycled for 3 cycle in the range 3.0–4.8 V and finally charged to 4.8 V, diffraction pattern resembled that of initial phase and was indexed with

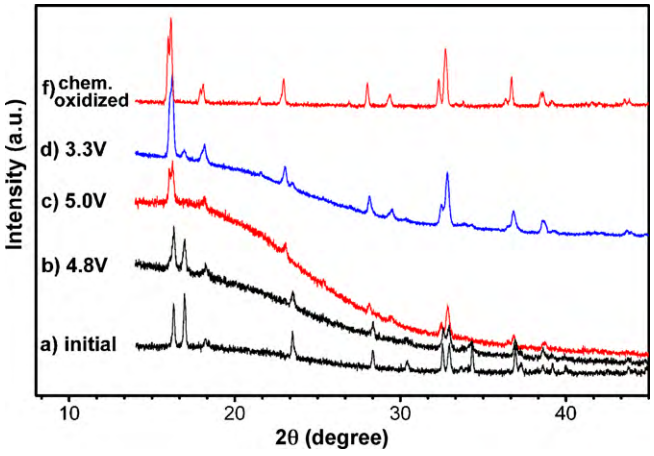

Fig. 4. Evolution of XRD pattern for Li_2CoPO_4F upon electrochemical cycling. Diffraction patterns of electrodes with different cycling profiles: a) initial phase, b) electrode charged to 4.8 V after 3 complete cycles in the range 3.0–4.8 V, c) electrode charged to 5.0 V, d) electrode discharged to 3.3 V after 7 complete cycles in the range 3.0–5.1 V, and f) chemically oxidized phase. The broad nature in the background at lower 2θ observed for electrodes is due to the mylar film.

Table 1
Results of *ex situ* XRD experiments presented in Fig. 4. Cell parameters for Li_2CoPO_4F electrode material charged to different potentials were refined in *Pnma* space group.

	a (Å)	*b* (Å)	*c* (Å)	*V* (Å^3)
Pristine compound	10.452(2)	6.3911(8)	10.874(2)	726.4(3)
Charged to 4.8 V	10.446(3)	6.3591(13)	10.854(3)	721.0(6)
Charged to 5.0 V	10.855(5)	6.271(2)	11.018(6)	752.1(8)
Discharged to 3.3 V	10.933(3)	6.2815(13)	11.048(2)	758.7(5)

Table 2
Structure refinement results of the chemically delithinated $Li_{1.75}Ni_{0.75}Fe_{0.25}PO_4F$ phase.

Atom	Site	x	y	z	U_{iso}/ Å^2
M1[a]	4a	0	0	0	0.0187(10)
M2[a]	4b	0.5	0	0	0.0202(12)
Li1[b]	8d	0.228(3)	0.465(4)	0.854(2)	0.044(2)
Li2	4c	0.732(3)	0.25	0.427(3)	0.044(2)
Li3	4c	0.448(2)	0.25	0.747(3)	0.044(2)
P1	4c	0.4657(4)	0.25	0.2472(6)	0.033(2)
P2	4c	0.2436(5)	0.25	0.0681(5)	0.033(2)
O1	8d	0.1798(4)	0.9518(8)	0.0207(4)	0.030(3)
O2	4c	0.2361(8)	0.75	0.2077(7)	0.030(3)
O3	4c	0.3169(6)	0.25	0.2427(9)	0.030(3)
O4	4c	0.3789(7)	0.75	0.0292(7)	0.030(3)
O5	4c	0.5034(9)	0.25	0.3691(8)	0.030(3)
O6	8d	0.4998(6)	0.4989(9)	0.1842(4)	0.030(3)
F1	4c	0.8848(6)	0.25	0.5337(5)	0.020(3)
F2	4c	−0.0414(5)	−0.25	0.1131(6)	0.020(3)

Orthorhombic, space group *Pnma* (No. 62), $Z = 8$, $a = 10.8907(1)$ Å, $b = 6.1549(1)$ Å $c = 11.0102(7)$ Å, and $V = 738.0(3)$ Å^3. Refinement parameters $R_I = 0.044$, $R_p = 0.0114$, $R_{wp} = 0.0149$, and GOF = 1.46.
[a] M, $Ni_{0.75}Fe_{0.25}$.
[b] Occupation factor $q = 0.75$.

cell parameters $a = 10.446(3)$ Å, $b = 6.3591(13)$ Å and $c = 10.854(3)$ Å (Fig. 4b). Observed decrease of the cell parameters was consistent with partial cobalt oxidation caused by the Li-extraction (Table 1) and suggested solid-solution behavior of the Li_2CoPO_4F phase upon charging up to 4.8 V.

Remarkable changes in the X-ray diffraction patterns were detected for the electrodes cycled to higher potentials, and XRD pattern of the electrode charged up to 5.0 V was evidently different from that of the pristine compound (Fig. 4c). Similar changes in XRD pattern were found for the electrode that was discharged to 3.3 V after 7 complete cycles between 3.0 and 5.1 V (Fig. 4d). These results clearly demonstrated that upon charging to potentials higher than 4.8 V there is no continuous evolution of the Li_2CoPO_4F structure, but in contrast a structural transformation takes place. Direct characterization of a new structure was impossible due to poor quality of diffraction patterns obtained *ex situ*, therefore structural exploration was carried out using XRD data collected for the sample oxidized chemically.

Attempts to oxidize Li_2CoPO_4F by nitrosonium nitrate were unsuccessful because of the high redox potential of the Co^{2+}/Co^{3+} couple, therefore chemical oxidation of iron-substituted fluorophosphates, $Li_2(M,Fe)PO_4F$ (M = Ni, Co), was undertaken. The presence of iron with the redox potential of the Fe^{2+}/Fe^{3+} couple much lower than that of the Co^{2+}/Co^{3+} one expected to enable chemical extraction of lithium from fluorophosphates, and thereby to induce structure transformation similar to that observed upon electrochemical delithiation. For this purpose single-phase $Li_2Ni_{0.75}Fe_{0.25}PO_4F$ sample ($a = 10.442(3)$ Å, $b = 6.332(2)$ Å, $c = 10.8368(3)$ Å, $V = 716.6(4)$ Å^3) was chosen. In contrast to $Li_2(Co,Fe)PO_4F$ samples the impact of fluorescence on X-ray diffraction data of $Li_2Ni_{0.75}Fe_{0.25}PO_4F$ was negligible, and its quality was sufficient for structure refinement. Upon chemical oxidation the color of $Li_2Ni_{0.75}Fe_{0.25}PO_4F$ was changed from gray to greenish, and essential modifications were detected on XRD pattern (Fig. 5). After careful examination the diffraction data were entirely indexed in the space group *Pnma* with cell parameters $a = 10.891(2)$ Å, $b = 6.151(2)$ Å, $c = 11.006(2)$ Å, which corresponded to a unit cell volume $V = 737.3(4)$ Å^3 superior to that of the pristine compound. The XRD pattern of the oxidized $Li_2Ni_{0.75}Fe_{0.25}PO_4F$ sample resembled those of the Li_2CoPO_4F electrodes charged to high potentials, and was used for structure refinement. It should be noted that recently we have succeeded to oxidize Li_2CoPO_4F using stronger oxidizer ($NO_2CF_3SO_3$), its XRD pattern is consistent with that of electrode charged up to 5.0 V (Fig. 4c and f).

The structure of the oxidized $Li_2Ni_{0.75}Fe_{0.25}PO_4F$ phase was elucidated by Rietveld method with the structural data of Li_2NiPO_4F applied as an initial model. The cell consisted of two independent metal sites randomly occupied by Ni (0.75) and Fe (0.25), three independent lithium sites, two phosphorous sites, six and two positions filled by oxygen and fluorine respectively. The atomic displacement parameters of lithium, phosphorous, oxygen and fluorine atoms were constrained to be equal for sites occupied by particular element. Because of the low scattering factor of lithium for X-rays the occupation factors of all Li-sites were fixed at value of 1.0 at initial stages of refinement and allowed to be refined at the last steps. For the Li(2) and Li(3) sites they appeared to be close to 1.0, while occupation of the Li(1) site was refined to be 0.70(2). This value was rather close to value of 0.75, expected for the investigated sample upon complete oxidation of Fe^{2+} to Fe^{3+} resulting in composition of $Li_{1.75}Ni_{0.75}Fe_{0.25}PO_4F$. This finding (Li-removal from the Li(1) site) agreed with suggestion of facile migration of weakly bonded lithium ions located at this site, and at the final stage of the refinement the occupation factor of Li1 was fixed at 0.75. Nevertheless, this assumption needs additional proofs, since redistribution of lithium ions between Li1 and Li2 positions should not be excluded. Structure parameters and reli-

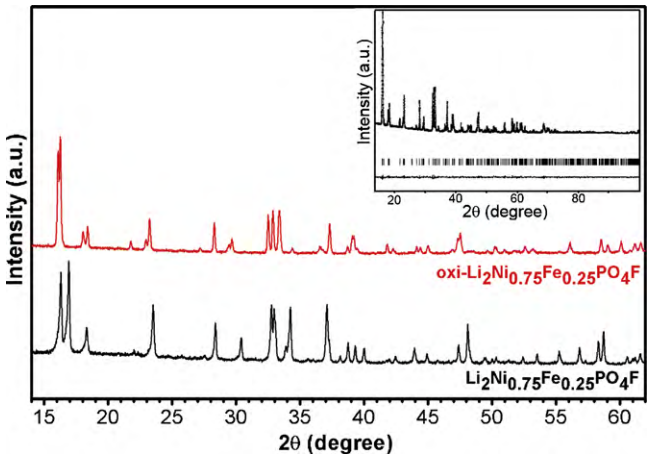

Fig. 5. XRD patterns of the pristine and chemically delithinated $Li_2Fe_{0.25}Ni_{0.75}PO_4F$ materials. Insert shows the final Rietveld plot with experimental data, calculated patterns difference curve and Bragg positions (vertical bars) of oxidized $Li_{1.75}Fe_{0.25}Ni_{0.75}PO_4F$.

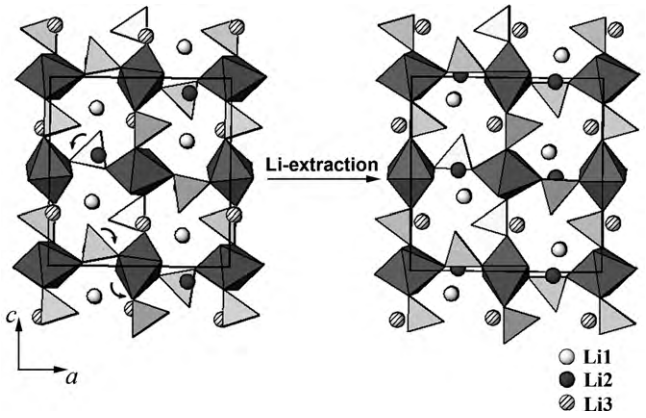

Fig. 6. Schematic representation of the structure transformation of Li_2MPO_4F upon Li-extraction. The projection along the *b*-axis is shown; arrows indicate rotation of structural units.

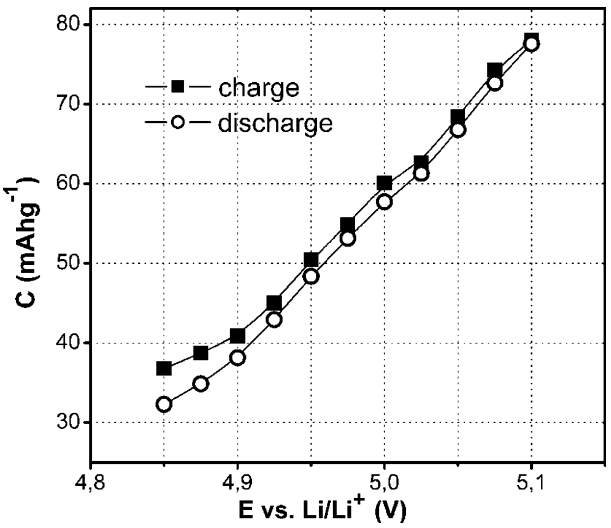

Fig. 7. Capacity vs. voltage obtained from potentiostatic step measurements between 4.2 V and variable anodic potentials. Polarization for 12 h was applied; values of current transients were corrected for residual currents.

ability factors obtained from the refinements are summarized in Table 2. The insert of Fig. 5 shows a representative experimental XRD pattern along with pattern obtained by Rietveld refinement for the delithiated $Li_2Ni_{0.75}Fe_{0.25}PO_4F$.

According to results of Rietveld refinement the 3D framework built of (MO_4F_2) octahedra and (PO_4) tetrahedra is preserved in the delithiated phase. However the Li-removal involves the mutual rotations of (MO_4F_2) octahedra and (PO_4) tetrahedra which accompanied by significant changes in the unit cell parameters. Whereas the *b* parameter is decreased, the *a* and *c* parameters are increased, that results in the volume expansion of >3.5%. Schematically structure modification is given in Fig. 6, where projection of pristine and delithiated structures along the *b*-axis are drawn. The anisotropy in lattice parameters variation can be explained by the structural features of Li_2MPO_4F. Upon oxidation of transition metal caused by the Li-extraction chains of edge-shared (MO_4F_2) octahedra running along [0 1 0] are compressed, and the *b* parameter is decreased. The compression of octahedra is accompanied by rotations of (MO_4F_2) octahedra as well as by rotations of (PO_4) groups occurring in the *ac*-plane, that increase the both *a* and *c* parameters. XRD pattern of Li_2CoPO_4F electrodes charged to different potentials were treated using results described above (Table 1). According to XRD data, Li_2CoPO_4F shows two distinct lithium extraction/reinsertion processes. Upon charging to potentials $\leq$4.8 V extraction of lithium takes place within the framework of the pristine phase, while extraction of larger amount of lithium upon charging to high potentials (>4.8 V) results in the structural transformation. This transformation is accompanied by the volume increase and appears to be irreversible: the subsequent insertion of lithium does not result in complete restoration of the initial structure, but takes place within the "modified" framework. These structural features might be explained by incomplete Li-restitution to the structure and redistribution of lithium ions over three possible crystallographic positions, and will be clarified by combination of neutron diffraction and NMR studies. It is interesting to note that this structure "modification" accompanied by the volume increase is expected to favor the migration of Li ions, because the wider interstitial space should support a faster lithium transport.

To estimate the steady-state capacity value we applied potentiostatic charge-discharge mode with starting potential 4.2 V and continued polarization at variable anodic potential (4.85–5.1 V) for 12 h, when the residual current remained time-independent (Fig. 7). After each step the potential discharge curve at 4.2 V was measured for the same time, and the value of residual current at 4.85–5.1 V was used to correct the observed current transients: subtraction of this current resulted in less than 15% decrease of the total charge. It should be noted that polarization of freshly prepared electrode at 4.85 V for 12 h resulted in complete structure transformation confirmed by additional electrochemical measurement followed by X-ray diffraction. The behavior observed at potentials >4.8 V is typical for solid-solutions, that agrees well with the results of *ex situ* XRD experiments (Table 1). The slope of the capacity–voltage dependence derived from the potentiostatic step measurements (about 0.7 V per 1Li mole) is close to that one observed for $LiCoO_2$ [24], this allows us to suggest that the complete extraction of one mole of lithium from Li_2CoPO_4F should occur at potentials ~5.5 V. The obtained data should be considered as preliminary, the complete evaluation of the Li_2CoPO_4F phase will be done by electrochemical measurements in electrolytes of higher anodic limit.

4. Conclusions

Electrochemical performance and structural properties of the high-voltage cathode material Li_2CoPO_4F have been investigated in the 3.0–5.1 V potential range. The most remarkable feature found for this material is the irreversible structure transformation, occurring upon Li-extraction at potentials > 4.8 V, with subsequent Li-extraction/insertion taking place within the "modified" framework. The structural transformation involves mutual rotations of (MO_4F_2) octahedra and (PO_4) tetrahedra accompanied by the unit cell expansion (>3.5%) which is expected to enhance Li-transport in the modified framework. This finding is in contrast to the volume contraction (about 7%) observed in the $LiCoPO_4$ phase for the complete lithium removal [22]. The irrevocable structure modification does not suppress, but is supposed to favor Li ion-migration upon subsequent Li-extraction/insertion. Therefore, extraction of lithium at initial steps might be considered as a "fine structure tuning" which makes the Li_2CoPO_4F framework more suitable for Li-transport.

It was shown that the Li-extraction from the modified framework occurs in a solid-solution manner and exhibits almost linear dependence of capacity vs. voltage up to 5.1 V. The slope of the capacity–voltage dependence derived from the potentiostatic step measurements suggests the complete extraction of one mole of lithium from Li_2CoPO_4F at potentials ~5.5 V. The electrochemical behavior of the Li_2CoPO_4F phase is quite different from that reported for $LiCoPO_4$ where complete Li-extraction is accompanied by two plateaus and occurs in much narrow potential

range (4.8–5.0 V) [22,23]. The electrochemical performance of the Li_2CoPO_4F material is expected to be improved by optimization of interfacial reactivity and careful choice of electrolyte with high anodic limit. Future investigations of Li_2CoPO_4F including complete electrochemical characterization will help to make decisive conclusions about perspectives of this material on the practical application in rechargeable lithium-ion batteries.

Acknowledgments

The work was supported in part by Russian Foundation for Basic Research (RFBR grant 10-03-00970-a). The authors would like to thanks R.V. Shpanchenko for collecting X-ray powder data for structure refinement, V.A. Alyoshin and I.V. Morozov for the preparation of oxidizers, A.A. Kovalenko for the determination of particle size. The authors also thank G.A. Tsirlina and O.A. Petrij for their helpful discussions.

References

[1] A.K. Padhi, K.S. Nanjundaswamy, C. Masquelier, J.B. Goodenough, J. Electrochem. Soc. 144 (1997) 1188–1194.
[2] A.K. Padhi, K.S. Nanjundaswamy, C. Masquelier, S. Okada, J.B. Goodenough, J. Electrochem. Soc. 144 (1997) 2581–2586.
[3] N. Ravet, J.B. Goodenough, S. Besner, M. Simoneau, P. Hovington, M. Armand, ECS Fall Meeting, Hawaii, 1999.
[4] A. Yamada, S.C. Chung, K. Hinokuma, J. Electrochem. Soc. 148 (2001) A224.
[5] A.K. Padhi, V. Manivannan, J.B. Goodenough, J. Electrochem. Soc. 145 (1998) 1518–1520.
[6] K.S. Nanjundaswamy, A.K. Padhi, J.B. Goodenough, S. Okada, H. Otsuka, H. Arai, J. Yamaki, Solid State Ionics 92 (1996) 1–10.
[7] A.K. Padhi, K.S. Nanjundaswamy, C. Masquelier, J.B. Goodenough, J. Electrochem. Soc. 144 (1997) 2581–2586.
[8] A. Nyten, A. Abouirmrane, M. Armand, T. Gustafsson, J.O. Tomas, Electrochem. Commun. 7 (2005) 156–160.
[9] A. Abouimrane, M. Armand, N. Ravet, in: K. Zaghib, C.M. Julien, J. Prakash (Eds.), New Trends in Intercalation Compounds for Energy Storage and Conversation, The Electrochemical Society Inc., 2003, pp. 15–22.
[10] J. Baker, M.Y. Saidi, R.K.B. Gover, P. Burns, A. Bryan, J. Power Sources 174 (2007) 927–931.
[11] S.-C. Yin, P. Subramanya Herle, A. Huggins, N.J. Taylor, Y. Makimura, L.F. Nazar, Chem. Mater. 18 (2006) 1745–1752.
[12] B.L. Ellis, W.R.M. Makahonouk, Y. Makimura, K. Toghill, L.F. Nazar, Nat. Mater. 6 (2007) 749–753.
[13] N. Recham, J.-N. Chotard, L. Dupont, C. Delacourt, W. Walker, M. Armand, J.-M. Tarascon, Nat. Mater. 9 (2009) 68–74.
[14] N. Recham, J.-N. Chotard, J.-C. Jumas, L. Laffont, M. Armand, J.-M. Tarascon, Chem. Mater. 22 (2010) 1142–1148.
[15] B.L. Ellis, W.R.M. Makahnouk, W.N.R. Weetaluktuk, D.H. Ryan, L.F. Nazar, Chem. Mater. 22 (2010) 1059–1070.
[16] M. Dutreilh, C. Chevalier, M. El-Ghozzi, D. Avignant, J. Solid State Chem. 142 (1999) 1–5.
[17] O.V. Yakubovitch, O.V. Karimova, O.K. Melnikov, Acta Crystallogr. C 53 (1997) 395–397.
[18] S. Okada, M. Ueno, Y. Uebou, J. Yamaki, J. Power Sources 146 (2005) 565–569.
[19] K. Bramnik, H. Hibst, N. Khasanova, E. Antipov, A. Ivanischev, International patent WO 023129 A2 (2010).
[20] I.D. Brown, D. Altermatt, Acta Crystallogr. B 41 (1985) 244–247.
[21] S.-C. Yin, H. Grondey, P. Strobel, M. Anne, L.F. Nazar, J. Am. Chem. Soc. 125 (2003) 10402–10411.
[22] N.N. Bramnik, K. Nikolowski, C. Baentz, K.G. Bramnik, H. Ehrenberg, Chem. Mater. 19 (2005) 908–915.
[23] V. Nakayama, S. Goto, Y. Uchimoto, M. Wakihara, Y. Kitayama, Chem. Mater. 16 (2004) 3399–3401.
[24] K. Mizushima, P.C. Jones, P.J. Wiseman, J.B. Goodenough, Mater. Res. Bull. 15 (1980) 783–789.